Topological phase transitions captured in the set of reduced density matrices

Samuel Warren, LeeAnn M. Sager-Smith,* and David A. Mazziotti†
Department of Chemistry and The James Franck Institute, The University of Chicago, Chicago, Illinois 60637, USA

(Received 3 August 2023; revised 30 October 2023; accepted 30 November 2023; published 18 January 2024)

Topological phase transitions fall outside of the symmetry-breaking paradigm and therefore elude many traditional analytical methods. In particular, significant geometric features found in the set of reduced density matrices (RDMs) disappear in symmetry-preserving topological systems. By returning to the fundamental properties of phase transitions, such as the divergence of correlation length and energy surface discontinuities, we demonstrate that the set of RDMs captures the critical behavior of systems with topological order. We find signatures of the gapless transition in the discontinuous movement of the ground-state RDMs. Additionally, the correlation length divergence near critical points appears in the off-diagonal character of RDMs, which is quantified through spectral and linear fitting analyses. This framework generalizes the quantum information approach to RDM critical theory, allowing for classification and visualization of all of the phases of the system—both topological and trivial—in the convex set of RDMs.

DOI: 10.1103/PhysRevB.109.045134

I. INTRODUCTION

Topological phase transitions, transitions that do not break system symmetries, have garnered significant theoretical and experimental interest due to the robust zero-energy edge states found in topological phases [1,2]. These resilient states are used in topological light emitting devices to protect against fabrication defects [3–8]. Additionally, research into topological quantum memory and computing focuses on harnessing the robustness of these edge states to reduce errors [9–12]. Topological order has also been used to explain exotic experimental phenomena like the quantum, spin, and fractional Hall effects [13–18]. However, many of the traditional analytical methods for studying phase transitions rely on symmetry breaking and therefore fail to capture the behavior of topological transitions.

The study of the relationship between reduced density matrices (RDMs) and quantum phase transitions was initiated by Erdahl and Jin [19], who noted that RDMs in different phases lie in significantly different regions of the set of RDMs. Gidofalvi and Mazziotti [20] later studied the movement of the RDMs between the regions with respect to critical parameters in the Hamiltonian and found that, in the vicinity of the transitions, the RDM moves very rapidly with one or more critical parameters and in the thermodynamic limit the speed becomes discontinuous at the critical point [21,22]. This work was then followed by Zauner and Verstraete [23] who discovered that, in systems with symmetry-breaking phase transitions, the geometry of the set of RDMs has significant features, such as ruled lines and surfaces that appear on the boundary of the set, reflecting the degeneracy of the symmetry-broken ground states. These features convey, without any reference to the underlying Hamiltonian, where symmetry breaking occurs in the system [23]. However, it was soon recognized by Chen [24] that the set of RDMs for systems with topological phases does not exhibit some of these geometric features such as the ruled lines and surfaces because no symmetries are broken between the trivial and topological regions. To recover the descriptive power of the RDM approach, aspects of the RDM set other than the ruled surfaces must be considered.

In this paper, we demonstrate that diverging correlation length and nonsmooth energy surfaces, signatures of phase transitions, are captured by an RDM approach to phase transitions regardless of the presence of symmetry breaking. Energy-surface discontinuities appear in the discontinuous movement of the RDM across the set, and the divergence of correlation length can be detected in the structure of the individual matrices of the set. We show that a simple visual inspection of the change in the RDMs during a transition reveals the divergence of correlation length, demonstrating an advantage of RDMs over the full N-body wave function, which can often obfuscate the true behavior of the system [25,26]. Additionally, we show that linear and spectral analysis of the RDMs can quantify this correlation length divergence and that analysis of higher-order RDMs reveals the rapid changes in higher-order correlations near the critical region [27–34].

To demonstrate this approach, we study the Su-Schrieffer-Heeger [35] and Kitaev chain models [36], two simple and extensively studied systems that exhibit topological edge states. The latter model adds the additional novelty of Majorana fermionic edge modes, which have garnered significant interest for their non-Abelian statistics but have had limited study in the field of RDM mechanics. These examples show that significant information about topological phase and multistate phenomena—e.g., gap closing—is captured entirely within the ground-state set of RDMs.

II. THEORY

For any Hamiltonian parameter space, the ground-state RDMs form a convex set. In the presence of symmetry-

*Present address: Department of Chemistry and Physics, Saint Mary's College, Notre Dame, Indiana 46556, USA.
†damazz@uchicago.edu

breaking phase transitions, distinct geometric features like ruled lines or surfaces begin to appear on the hull, the outer shell of the set, in the thermodynamic limit [23], reflecting the degeneracy of the symmetry-broken ground states. The benefit of this method is the simple visual identification of abstract concepts like symmetry breaking and the ability to visualize the entire phase space of the system in a finite convex set. However, this methodology fails to generate the same stark geometric features in the presence of topological phase transitions, where no symmetries are broken between the trivial and topological regions [24]. Other factors in the set of RDMs and the structure of the individual matrices must be considered to recover the descriptive power of this methodology.

Initial investigations of the link between critical phenomena and the set of 2-RDMs studied the movement of the RDMs near critical points. As the parameters of a Hamiltonian are varied, its ground-state RDMs move along the convex hull, and the speed or one of the higher derivatives of this parametric curve becomes discontinuous near symmetry-breaking quantum phase transitions [20–22]. This approach was then incorporated into Verstraete's geometric interpretation of the convex hull as a form of parametric curvature [23], expanding the analytical capability of both approaches. However, this connection between the two methods does not necessarily subject the speed or other Hamiltonian-dependent metrics to the same constraints as the ruled-surfaces approach when studying topological phases.

The movement of the RDMs arises from the changes in all one- and two-particle expectation values,

$$\frac{\partial^n r}{\partial \mathbf{t}^n} = \sqrt{\sum_i \left(\frac{\partial^n O_i}{\partial \mathbf{t}^n}\right)^2}, \tag{1}$$

where O_i is the ith observable varied by the parameter(s) $\mathbf{t}$, and r is a coordinate for the RDMs within the convex set. As the Hamiltonian is a weighted sum of these observables, the behavior of the energy is intimately tied to the movement of the RDM. Near critical points, the system's energy or its higher derivatives become discontinuous despite the parameters changing continuously. Therefore, the observables are discontinuous, and thus, the movement of the RDMs must also become discontinuous.

In the case of topological phase transitions, each transition is associated with a closing of the band gap. This closing, along with the spontaneous generation of zero-energy edge modes, introduces discontinuities into the energy surface near the critical points. These discontinuities are then also found in the speed or higher derivatives of the RDMs. The speed, however, relies on knowledge of the Hamiltonian and its parameters, which are not needed in the symmetry-broken geometric analysis of the set of RDMs. A more Hamiltonian-agnostic approach to analyzing topological phase transitions with RDMs requires the investigation of other properties of RDMs in order to abstract the set from the system parameters.

The universality of phase transitions arises due to the divergence of correlation lengths near critical points. In topological insulating systems the correlation length directly coincides with the edge-state decay length [37]. This decay length is how far the edge states penetrate into the bulk of the material in the topological phase. If these edge states are Dirac fermions, they can be described as a linear combination of creation operators acting on the vacuum state and are, therefore, natural orbitals of the 1-particle RDM (1-RDM)

$$^1D^i_j = \langle \Psi | \hat{a}^\dagger_i \hat{a}_j | \Psi \rangle , \tag{2}$$

where $\hat{a}^\dagger_i$ and $\hat{a}_i$ are the ith fermionic creation and annihilation operators, $|\Psi\rangle$ is the N-body fermionic ground-state wave function, and ^1D is the 1-RDM. Therefore near the critical points, when the edge states are bleeding considerably into the bulk, more off-diagonal elements of the RDM will have finite values with the RDM becoming maximally off-diagonal at the point of the transition as the edge states collapse into the bulk.

The RDM approach to topological phase transitions can be generalized to quadratic Hamiltonians, with the study of the 2-RDM

$$^2D^{ij}_{kl} = \langle \Psi | \hat{a}^\dagger_i \hat{a}^\dagger_j \hat{a}_l \hat{a}_k | \Psi \rangle . \tag{3}$$

Quadratic Hamiltonians can contain additional non-particle-conserving terms which do not appear in the 1-RDM, but result in strong 2-body correlation. While the 2-RDM contains additional information, it also contains information that is redundant with the 1-RDM. In order to demonstrate the contribution of these non-particle-conserving terms to the edge modes, it is possible to subtract the 1-RDM contributions from the 2-RDM leaving behind the cumulant part of the 2-RDM [38,39]:

$$^2\Delta = {}^2D - {}^1D \wedge {}^1D, \tag{4}$$

where $\wedge$ is the Grassmann wedge product [40] and $^2\Delta$ is the two-particle cumulant. The largest eigenvector and value of the cumulant has been used extensively to demonstrate fermion-fermion [31,41–43] and fermion-hole [44] correlation, pairing, and condensation in systems. Therefore, as a measure of correlation, the eigenvalue should experience significant changes as the system approaches a critical point due to the divergence of correlation length.

An additional metric that can be used to study both the 1- and 2-RDMs is the Pearson correlation coefficient (PCC), which can quantify the degree to which a matrix is diagonal. The PCC has also been used to study the time correlation between blocks of the RDMs and their cumulants [45]. In general, the PCC determines the degree of linear or antilinear correlation between two sets of data, with a value between 1 (if the data lie along a line with a positive slope) or -1 (if the data lie along a line with a negative slope) and a value of 0 signifying no linear correlation between the two data sets.

This metric can also be used to determine the diagonal character of a matrix by measuring the correlation between the rows and columns. The elements of the RDM, being a density matrix, give a measure of the probability of two events (the column and row operators) occurring in the system. This suggests the following form of the PCC:

$$\frac{n\langle ij\rangle - \langle i\rangle \langle j\rangle}{\sqrt{n\langle i^2\rangle - \langle i\rangle^2}\sqrt{n\langle j^2\rangle - \langle j\rangle^2}}, \tag{5}$$

where for the 1-RDM

$$n = \sum_{i,j}^{N} |\langle \hat{a}_i^\dagger \hat{a}_j \rangle|, \langle i \rangle = \sum_{i,j}^{N} i |\langle \hat{a}_i^\dagger \hat{a}_j \rangle|,$$

$$\langle ij \rangle = \sum_{i,j}^{N} ij |\langle \hat{a}_i^\dagger \hat{a}_j \rangle|.$$

Due to the Hermitian nature of RDMs, this can be simplified to

$$\frac{n\langle ij \rangle - \langle i \rangle^2}{n\langle i^2 \rangle - \langle i \rangle^2}, \tag{6}$$

where it can easily be seen that a diagonal matrix in which $\langle ij \rangle = \langle i^2 \rangle$ will have a PCC value of 1. Conceptually, the 1-RDM element $\hat{a}_i^\dagger \hat{a}_j$ gives a measure of how often the system transitions from a state where there is a particle at site j and no particle at site i to a state with the opposite particle filling at sites j and i. Thus, the absolute values of the elements can be thought of as the unnormalized frequency of these events. The PCC can then be used to measure the linear correlation between this series of pairs of events. Taking the case of a pure insulator, e.g., a chain of very distantly separated hydrogen atoms, the expected structure of the 1-RDM is entirely diagonal; thus, the PCC should be equal to 1. However, if a system contains a topological phase transition, the coupling between the edges and the bulk should result in a drastic drop in the PCC value when the band gap closes.

III. RESULTS

This section analyzes the Su-Schrieffer-Heeger (SSH) and the Kitaev chain topological systems. First, the structure of the 1-RDMs is investigated, revealing the visual signature of topological edge states. Then the speed and off-diagonal character of the RDMs are analyzed as the system travels through a topological phase transition. Finally, in the Kitaev chain model, due to its non-number-conserving terms, the cumulant of the system can be analyzed, revealing the significance of 2-particle correlation in the topological transition.

A. SSH model

One of the simplest systems with topological order is the Su-Schrieffer-Heeger model [35], which has garnered attention due to its experimental application in topological lasers [3,7]:

$$\hat{H} = v \sum_{i=1}^{N} \hat{a}_{2i-1}^\dagger \hat{a}_{2i} + w \sum_{i=1}^{N-1} \hat{a}_{2i}^\dagger \hat{a}_{2i+1} + \text{H.c.}, \tag{7}$$

where N is the number of particles in a half-filled chain, v and w are real parameters, H.c. denotes Hermitian conjugate, and the finite $2N$-site chain is treated without periodic boundary conditions. The first term in the Hamiltonian is block diagonal with blocks of $\sigma_x = \left(\begin{smallmatrix} 0 & 1 \\ 1 & 0 \end{smallmatrix}\right)$. Therefore, 1-particle solutions, when $|v| \gg |w|$ (far into the *trivial region*), are of the form

$$|\Psi_i\rangle = \frac{1}{\sqrt{2}} (\hat{a}_{2i-1}^\dagger \pm \hat{a}_{2i}^\dagger) |\varnothing\rangle , \tag{8}$$

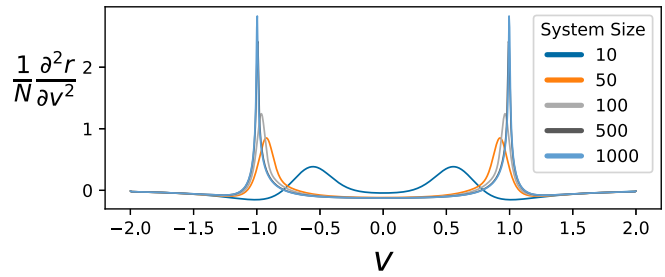

FIG. 1. RDM acceleration through a topological phase transition in the SSH model. The acceleration is calculated using Eq. (1), and is divided by the system size for normalization. The results are for the ground-state RDM for a system that is tuned from $[v, w]$: $[-2, -1] \rightarrow [2, -1]$ [see Eq. (7)] passing through 2 phase transitions at $v = \pm 1$.

in which $|\varnothing\rangle$ is the vacuum state. The second term in the Hamiltonian is identical in the bulk of the material (aside from a shift up by 1 in the indices), but possesses two additional diagonal elements at the edges with eigenvalues of 0. These zero-energy edge states,

$$|\Psi_0\rangle = \frac{1}{\sqrt{2}} (\hat{a}_1^\dagger \pm \hat{a}_{2N}^\dagger) |\varnothing\rangle , \tag{9}$$

appear in the *topological region* ($|w| > |v|$).

The ground-state RDM's movement can be tracked as the system is taken through a topological phase transition. Figure 1 displays the normalized acceleration of the ground-state RDM for various system sizes. This is calculated using Eq. (1), which for this system can be explicitly expressed as

$$\frac{\partial^2 r}{\partial t^2} = \sqrt{\left(\frac{\partial^2 r_w}{\partial w^2}\right)^2 + \left(\frac{\partial^2 r_v}{\partial v^2}\right)^2}, \tag{10}$$

where

$$r_w = \langle \Psi(w, v)| \sum_{i=1}^{N} (\hat{a}_{2i-1}^\dagger \hat{a}_{2i} + \text{H.c.}) |\Psi(w, v)\rangle \tag{11}$$

and

$$r_v = \langle \Psi(w, v)| \sum_{i=1}^{N-1} (\hat{a}_{2i}^\dagger \hat{a}_{2i+1} + \text{H.c.}) |\Psi(w, v)\rangle . \tag{12}$$

The acceleration was chosen, as it is the lowest derivative of the movement that becomes discontinuous near the critical point, likely due to the curvature of the energy diverging near the gap closing. Even at small system sizes, significant changes in the acceleration of the RDM can be seen with the curves converging on a similar structure as the number of sites grows. Near $|v| = 1$, the acceleration begins to change rapidly with larger systems exhibiting a larger normalized change, indicating that a phase transition would occur at this point in the thermodynamic limit. Therefore, the movement of the RDMs along the convex set continues to function as a useful parameter for finding both topological and symmetry-breaking phase transitions.

The transition between the topological and trivial regions can also be observed in the structure of the 1-RDMs as seen in Figs. 2(a), 2(b), and 2(c). In the trivial region, presented in

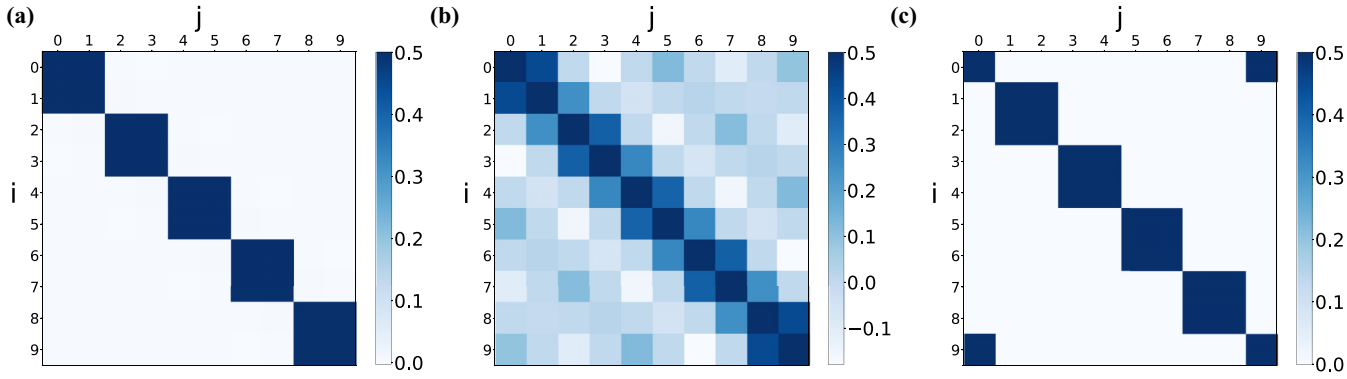

FIG. 2. Structural changes in the 1-RDM near topological phase transition in the SSH Hamiltonian. Panels (a)–(c) show the matrix elements of the 1-RDMs for a 10-site system in the trivial ($100v = w$), gapless ($v = w$), and topological ($v = 100w$) phases, respectively, where each matrix element is given by $\langle \hat{a}_i^\dagger \hat{a}_j \rangle$.

Fig. 2(a), the block-diagonal structure of the 1-RDM shows that it is energetically favorable for pairs of neighboring sites to bind tightly together, and demonstrates the extremely local nature of the correlation in the system. At the transition point between the two phases, the gap closes, the material becomes conductive, and the correlation or, equivalently, the edge state decay length reaches its maximum. This is reflected in Fig. 2(b) where connections form between all of the neighbors dissolving the block-diagonal structure. Finally, in the topological region, presented in Fig. 2(c), there is the same insulating behavior in the bulk of the material that is observed in the trivial region, but now there exist distinct and highly visible connections between the edges of the chain, demonstrating how edge states are easily visualized in an RDM-based framework.

This off-diagonal character can be measured through the use of the PCC. Figure 3 shows the value of the PCC as the system is taken from the trivial region into the topological and back out again for varying particle number. As the particle number increases, a discontinuity appears to form in the PCC value at the exact point of the phase transition, $v = 1$. This discontinuity reflects the sudden increase in correlation length that occurs near a critical point. Interestingly, even in the low-particle limit (10 particles), taking the derivative

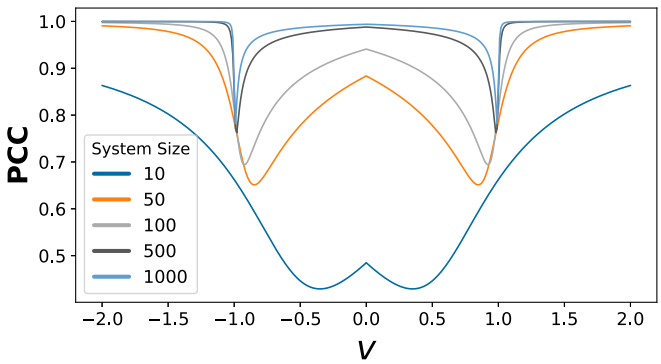

FIG. 3. Change in the Pearson correlation coefficient near topological phase transitions in the SSH Hamiltonian. The Hamiltonian is tuned from $[v, w]$: $[-2, -1] \rightarrow [2, -1]$ [see Eq. (7)] passing through two phase transitions at $v = \pm 1$.

of the PCC with respect to v reveals that the PCC changes most rapidly exactly at $v = 1$, indicating that this metric is incredibly sensitive to the gap closing even before the system approaches the thermodynamic limit. This plot also shows a discontinuity in the derivative of the PCC at $v = 0$, which disappears with increasing system size. By using a nonsmooth function like the absolute value of the RDM elements in the calculation of the PCC, when the sign of the elements flip, like at $v = 0$, a discontinuity occurs in the PCC.

This "single particle" system generates ground states that are completely captured in the 1-RDM making the higher-order RDMs trivial and redundant. The next system, however, introduces two-particle correlations that complicate a purely 1-RDM based analysis.

B. Kitaev chain

The Kitaev chain was developed as a simple system that can not only demonstrate topological order, but also produce Majorana edge modes (MEMs) [36]. The non-Abelian statistics of these MEMs make them very appealing for quantum computing applications where they may protect against the intrusion of noise. Pairs of MEMs are defined as

$$\hat{m}_{2i} = \hat{a}_i + \hat{a}_i^\dagger, \tag{13}$$

$$\hat{m}_{2i+1} = -i(\hat{a}_i - \hat{a}_i^\dagger), \tag{14}$$

which obey the anticommutation relationship $\{\hat{m}_i, \hat{m}_j\} = 2\delta_{ij}$ [46]. In order to obtain these states, Kitaev generated a Hamiltonian similar to the SSH chain, except that MEMs instead of Dirac fermions form on the edge.

The Hamiltonian can be written in terms of Dirac fermionic operators,

$$\hat{H} = \sum_i \mu \hat{a}_i^\dagger \hat{a}_i + \omega(\hat{a}_i^\dagger \hat{a}_{i+1} + \text{H.c.}) + \beta(\hat{a}_i \hat{a}_{i+1} + \text{H.c.}), \tag{15}$$

where the first term is a chemical potential, the second term is a nearest-neighbor hopping interaction, and the final term represents the superconducting gap. We will use $\hat{\mu}$, $\hat{\omega}$, and $\hat{\beta}$ to denote the operators found in the first, second, and third terms of the Hamiltonian. The cumulant eigenvectors for systems up to 18 sites are calculated through the exact diagonalization

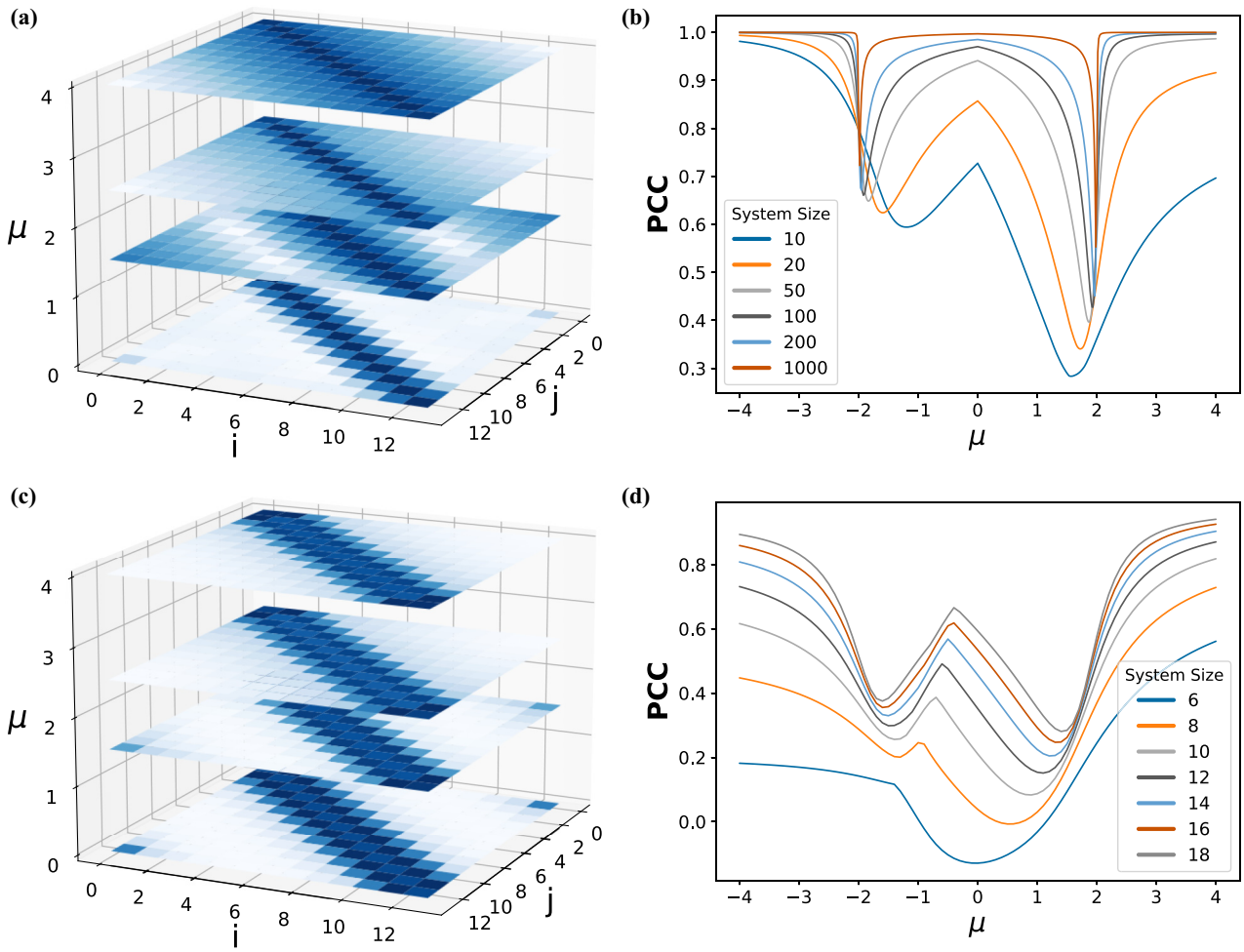

FIG. 4. Signatures of topological phase transitions in the structure of the 1-RDM and the 2-particle cumulant in the Kitaev chain model. Panel (a) shows the change in the structure of the 1-RDM as it is taken through a topological phase transition at $\mu = 2$ (to emphasize the shift of population to the edges, the color scale of the RDM element is logarithmic in base 10), and panel (b) shows how this change is reflected in the PCC. Panel (c) shows the changes in the structure of the eigenvector of the largest eigenvalue of the 2-particle cumulant (LCE) [see Eq. (17)], and panel (d) shows the PCC of the LCE as the system is taken through the same phase transitions. All of the plots have $[\omega, \beta] = [-1, -1]$ [see Eq. (15)].

of the Hamiltonian, while through the use of the Bogoliubov transform it is possible to obtain the 1-RDM's for systems on the order of 1000 particles. We can also use the Bogoliubov transform to obtain the spectra:

$$e(k) = \pm\sqrt{(2\omega\cos k + \mu)^2 + 4\beta^2 \sin^2 k} \quad -\pi \leqslant k \leqslant \pi, \tag{16}$$

where k is a wave vector. This equation shows that there are two gapped regions separated by the gapless line $\mu = -2\omega$. The first and second regions occur (a) when $|\mu| > 2|\omega|$ and (b) when $2|\omega| > |\mu|$ with $\beta \neq 0$, respectively. Additionally, another gapless line can be found when $\beta = 0$ in (b). This bulk analysis does not reveal which region contains the MEMs, but these can be found by analyzing the RDMs in the various regions.

The 1-RDMs shown in Fig. 4(a) are from the path μ: $0 \rightarrow 4$, $\beta/\omega = 1$ for a system with 14 sites. In the regime of large (absolute value) μ all the way to slightly above ($\mu = 2.5$) there are no apparent edge states. The tridiagonal nature of the 1-RDMs also shows the relatively short correlation length scale of the system. However, immediately after the transition at $\mu = 2$, the edge states begin to appear, and more off-diagonal elements become populated indicating the divergence of length scales near the critical point. Finally, deep in the topological region when $\mu = 0$, the edge states peak with an apex at $|.25|$ and the local tridiagonal nature of the bulk returns.

Figure 4(b) shows the sharpening of the transition through the PCC value for the 1-RDM as the particle number increases. The PCC value for the different system sizes changes rapidly, with larger systems converging to a structure that diverges at $\mu = 2$, serving as a signature of a topological transition. Additionally, the discontinuity due to the measurement of absolute values of the 1-RDM elements is seen at $\mu = 0$. Like the SSH model, the derivative of the PCC with respect to μ shows a peak at the $\mu = 2$ even at 10 particles, but unlike the SSH model a significant asymmetry with respect to μ has appeared. This is likely caused by the rapid drop in particle number in regions with positive chemical potential values. Therefore, the edge modes contribute more to the

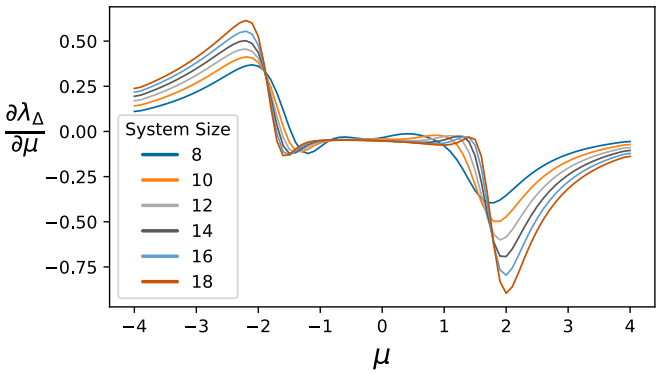

FIG. 5. Changes in the largest cumulant eigenvalue near topological phase transitions in the Kitaev chain. The legend depicts the size of the system for 8–18 site systems as the Hamiltonian is tuned from $[\mu, \omega, \beta]$: $[-4, -1, -1] \rightarrow [4, -1, -1]$ [see Eq. (15)].

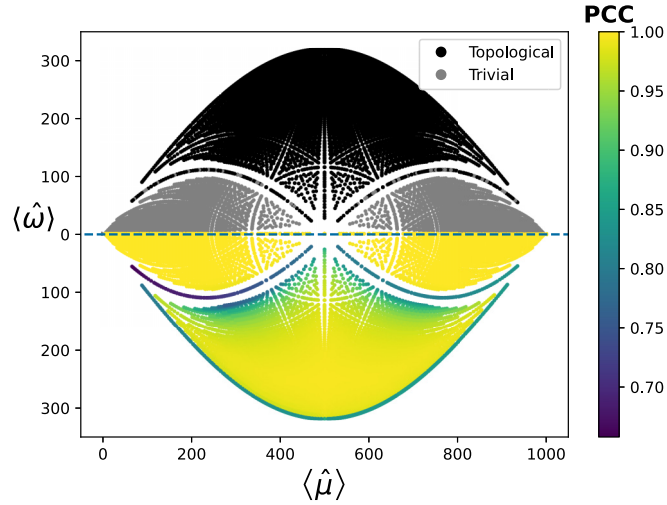

FIG. 6. Slice of the convex set of the ground-state RDMs of the Kitaev chain model. For this 1000-site system, the coloring of this figure is split around the gray dashed line, where the upper half is a binary coloring with gray or black indicating that a point lies in the trivial or topological regimes, respectively. In the lower half, the coloring corresponds to the color bar to the right and depicts the value of the PCC [see Eq. (5)] at any point. $\langle\hat{\omega}\rangle$ and $\langle\hat{\mu}\rangle$ refer to the expectation value of Hamiltonian terms found in Eq. (15).

overall behavior of the 1-RDM, being a larger percentage of the population of the system than in the particle-rich region.

This 1-RDM analysis, however, ignores the newly added 2-body correlation, which can be found in the 2-particle cumulant. The eigenvector associated with the largest eigenvalue of the cumulant (LCE) gives a picture of the most dominant 2-body effects in the system [42]. We define this eigenvector, g, as

$$\lambda_\Delta = g_{ij}^{\dagger\,2} \Delta_{kl}^{ij} g_{kl}, \tag{17}$$

where λ_Δ is the largest eigenvalue of the 2-particle cumulant. Then by plotting g_{ij}, we recover a plot similar to the plot of the 1-RDM, but this plot contains spatial information about 2-body correlations in the system. Looking at Fig. 4(c) in the region with $\mu > 2$, the large number of off-diagonal terms indicates that the LCE contains information about long-range order in the system arising from the superconducting gap term in the Hamiltonian. Interestingly, the cumulant displays an identical transformation to the 1-RDM with the formation of edge states at $\mu < 2$. However unlike the 1-RDM, in the exact MEM limit, $\mu = 0$, the edge state is not completely isolated with some contributions coming from elements near the edges (i.e., $\langle \hat{a}_0^\dagger \hat{a}_{N-1}^\dagger \rangle$, ...). Looking at Fig. 4(d), which is plotting the value of PCC for the LCE, aside from the 6-particle case, the values seem to follow a similar pattern to the RDM PCC curves. The peaks of the plots are lower due to the superconducting term generating nearly diagonal connections between the sites, but the linear correlation still experiences a significant drop near the phase transition. These rapid changes in correlation captured by this linear fitting can also be seen in a spectral analysis of the cumulant. The change in the eigenvalue of the LCE can be seen in Fig. 5. As a reflection of the divergence of correlation lengths when approaching the critical point, the eigenvalue changes very rapidly indicating that the two-particle correlation is undergoing a dramatic change.

Analysis of a slice of the convex set of RDMs provides a map of the phases of the system. Figure 6 displays a portion of the set for the 1000-site system mirrored around the horizontal dotted line, where above the line a binary color scale depicts the trivial region as gray and the topological as black, while below the line the color scale for the PCC can be seen in the color bar. The set was collected via sampling a grid in the Hamiltonian parameter space, which results in sparse regions that would likely be filled if the plot had been drawn with random sampling. This sparsity, however, is the result of the RDM moving rapidly near the phase transition, thus showing the divergence of the speed. This illustrates how speed information can be incorporated in the set picture. Finally, the value of the PCC also appears to fall at the site of the topological transition and near the bottom of the figure, reflecting the closing of the band gap that occurs at the transition and when $\beta = 0$. While it is not visible in this 2-D projection, there is also a significant gap in the RDMs between the yellow and green regions. This, of course, is not a topological phase transition, indicating that the PCC and speed might serve as a general indicator of when the gap is closing rather than a definitive sign of topological order.

IV. DISCUSSION AND CONCLUSIONS

Characterization of topological phases is a vitally important step in the development of novel technologies like topological transistors, lasers, and quantum computers. In this article, we introduce the RDM approach to topological phase transitions and analyze two simple systems exhibiting topological order. The first system, the SSH model, demonstrates that fermionic edge modes appear as easily recognizable features in the structure of the 1-RDM. Additionally, we see that the 1-RDM passes through a region with considerable off-diagonal character as the gap closes, reflecting the divergence of correlation length near critical points. The Pearson correlation coefficient (PCC), which spikes at the point of the gap closing, quantifies this off-diagonal quality by providing

a simple metric, untethered from the Hamiltonian parameters, for identifying phase transitions.

The next system, the Kitaev chain, presents a novel challenge for RDM theory in the form of Majorana fermions. We show, however, that these fermions appear in the 1-RDM and that the transition exhibits the same off-diagonal spiking, seen in the PCC, as the SSH transition. Using this behavior, we reconstruct a picture of the full set of RDMs, which easily distinguishes between the phases without any reference to the underlying Hamiltonian, a useful trait for experimental settings. The Kitaev chain also contains non-number-conserving particle terms, which introduce higher-order correlations to the system. This two-particle correlation is seen in the spectrum of the cumulant, and near the critical regions, the largest eigenvalue undergoes considerable shifts reflecting the divergence of correlation length scale.

These results demonstrate the power of the RDM approach to topological phase transitions, presenting a method that is able to resolve multistate phenomena like gap closing with ground-state information in an easily interpreted framework. This has many advantages not only for finite-sized theoretical modeling, but also for experiments or quantum computing simulations where calculation of the 1- and 2-RDMs requires considerably fewer measurements than complete determination of the wave function.

ACKNOWLEDGMENTS

D.A.M. gratefully acknowledges support from the U.S. National Science Foundation under Grant No. CHE-2155082 and the Department of Energy, Office of Basic Energy Sciences under Grant No. DE-SC0019215.

[1] D. J. Thouless, M. Kohmoto, M. P. Nightingale, and M. den Nijs, Quantized Hall conductance in a two-dimensional periodic potential, Phys. Rev. Lett. **49**, 405 (1982).

[2] F. D. M. Haldane, Model for a quantum Hall effect without Landau levels: Condensed-matter realization of the "parity anomaly", Phys. Rev. Lett. **61**, 2015 (1988).

[3] P. St-Jean, V. Goblot, E. Galopin, A. Lemaître, T. Ozawa, L. Le Gratiet, I. Sagnes, J. Bloch, and A. Amo, Lasing in topological edge states of a one-dimensional lattice, Nat. Photonics **11**, 651 (2017).

[4] M. A. Bandres, S. Wittek, G. Harari, M. Parto, J. Ren, M. Segev, D. N. Christodoulides, and M. Khajavikhan, Topological insulator laser: Experiments, Science **359**, eaar4005 (2018).

[5] Z.-K. Shao, H.-Z. Chen, S. Wang, X.-R. Mao, Z.-Q. Yang, S.-L. Wang, X.-X. Wang, X. Hu, and R.-M. Ma, A high-performance topological bulk laser based on band-inversion-induced reflection, Nat. Nanotechnol. **15**, 67 (2020).

[6] Y. Zeng, U. Chattopadhyay, B. Zhu, B. Qiang, J. Li, Y. Jin, L. Li, A. G. Davies, E. H. Linfield, B. Zhang, Y. Chong, and Q. J. Wang, Electrically pumped topological laser with valley edge modes, Nature (London) **578**, 246 (2020).

[7] T. H. Harder, M. Sun, O. A. Egorov, I. Vakulchyk, J. Beierlein, P. Gagel, M. Emmerling, C. Schneider, U. Peschel, I. G. Savenko, S. Klembt, and S. Höfling, Coherent topological polariton laser, ACS Photonics **8**, 1377 (2021).

[8] J. Tian, Q. Y. Tan, Y. Wang, Y. Yang, G. Yuan, G. Adamo, and C. Soci, Perovskite quantum dot one-dimensional topological laser, Nat. Commun. **14**, 1433 (2023).

[9] A. Y. Kitaev, Fault-tolerant quantum computation by anyons, Ann. Phys. **303**, 2 (2003).

[10] A. Kitaev, Anyons in an exactly solved model and beyond, Ann. Phys. **321**, 2 (2006).

[11] M. Freedman, C. Nayak, and K. Shtengel, Extended Hubbard model with ring exchange: A route to a non-Abelian topological phase, Phys. Rev. Lett. **94**, 066401 (2005).

[12] P. Fendley and E. Fradkin, Realizing non-Abelian statistics in time-reversal-invariant systems, Phys. Rev. B **72**, 024412 (2005).

[13] R. B. Laughlin, Quantized Hall conductivity in two dimensions, Phys. Rev. B **23**, 5632 (1981).

[14] A. H. MacDonald, Edge states in the fractional-quantum-Hall-effect regime, Phys. Rev. Lett. **64**, 220 (1990).

[15] S. Das Sarma, M. Freedman, and C. Nayak, Topologically protected qubits from a possible non-Abelian fractional quantum Hall state, Phys. Rev. Lett. **94**, 166802 (2005).

[16] M. Barkeshli and X.-G. Wen, Anyon condensation and continuous topological phase transitions in non-Abelian fractional quantum Hall states, Phys. Rev. Lett. **105**, 216804 (2010).

[17] E. Ardonne and K. Schoutens, New class of non-Abelian spin-singlet quantum Hall states, Phys. Rev. Lett. **82**, 5096 (1999).

[18] T. Senthil, J. B. Marston, and M. P. A. Fisher, Spin quantum Hall effect in unconventional superconductors, Phys. Rev. B **60**, 4245 (1999).

[19] R. M. Erdahl and B. Jin, The lower bound method for reduced density matrices, J. Mol. Struct (THEOCHEM) **527**, 207 (2000).

[20] G. Gidofalvi and D. A. Mazziotti, Computation of quantum phase transitions by reduced-density-matrix mechanics, Phys. Rev. A **74**, 012501 (2006).

[21] C. A. Schwerdtfeger and D. A. Mazziotti, Convex-set description of quantum phase transitions in the transverse Ising model using reduced-density-matrix theory, J. Chem. Phys. **130**, 224102 (2009).

[22] S. Warren, L. M. Sager-Smith, and D. A. Mazziotti, Quantum simulation of quantum phase transitions using the convex geometry of reduced density matrices, Phys. Rev. A **106**, 012434 (2022).

[23] V. Zauner, D. Draxler, L. Vanderstraeten, J. Haegeman, and F. Verstraete, Symmetry breaking and the geometry of reduced density matrices, New J. Phys. **18**, 113033 (2016).

[24] J.-Y. Chen, Z. Ji, Z.-X. Liu, Y. Shen, and B. Zeng, Geometry of reduced density matrices for symmetry-protected topological phases, Phys. Rev. A **93**, 012309 (2016).

[25] P.-O. Löwdin, Quantum theory of many-particle systems. I. Physical interpretations by means of density matrices, natural spin-orbitals, and convergence problems in the method of configurational interaction, Phys. Rev. **97**, 1474 (1955).

[26] P.-O. Löwdin, Quantum theory of many-particle systems. II. Study of the ordinary Hartree-Fock approximation, Phys. Rev. **97**, 1490 (1955).
[27] C. N. Yang, Concept of off-diagonal long-range order and the quantum phases of liquid He and of superconductors, Rev. Mod. Phys. **34**, 694 (1962).
[28] F. Sasaki, Eigenvalues of fermion density matrices, Phys. Rev. **138**, B1338 (1965).
[29] A. J. Coleman, The structure of fermion density matrices. III. Long-range order, J. Low Temp. Phys. **74**, 1 (1989).
[30] L. M. Sager and D. A. Mazziotti, Cooper-pair condensates with nonclassical long-range order on quantum devices, Phys. Rev. Res. **4**, 013003 (2022).
[31] T. Juhász and D. A. Mazziotti, The cumulant two-particle reduced density matrix as a measure of electron correlation and entanglement, J. Chem. Phys. **125**, 174105 (2006).
[32] J. E. Harriman, Reduced-density-matrix cumulants and correlation, Phys. Rev. A **75**, 032513 (2007).
[33] D. R. Alcoba, R. C. Bochicchio, L. Lain, and A. Torre, On the measure of electron correlation and entanglement in quantum chemistry based on the cumulant of the second-order reduced density matrix, J. Chem. Phys. **133**, 144104 (2010).
[34] E. Ramos-Cordoba, P. Salvador, and E. Matito, Separation of dynamic and nondynamic correlation, Phys. Chem. Chem. Phys. **18**, 24015 (2016).
[35] W. P. Su, J. R. Schrieffer, and A. J. Heeger, Solitons in polyacetylene, Phys. Rev. Lett. **42**, 1698 (1979).
[36] A. Kitaev, Unpaired Majorana fermions in quantum wires, Phys. Usp. **44**, 131 (2001).
[37] W. Chen, M. Legner, A. Rüegg, and M. Sigrist, Correlation length, universality classes, and scaling laws associated with topological phase transitions, Phys. Rev. B **95**, 075116 (2017).
[38] D. A. Mazziotti, Approximate solution for electron correlation through the use of Schwinger probes, Chem. Phys. Lett. **289**, 419 (1998).
[39] M. Bianucci and M. Bologna, About the foundation of the Kubo generalized cumulants theory: A revisited and corrected approach, J. Stat. Mech.: Theory Exp. (2020) 043405.
[40] D. A. Mazziotti, Contracted Schrödinger equation: Determining quantum energies and two-particle density matrices without wave functions, Phys. Rev. A **57**, 4219 (1998).
[41] J. T. Skolnik and D. A. Mazziotti, Cumulant reduced density matrices as measures of statistical dependence and entanglement between electronic quantum domains with application to photosynthetic light harvesting, Phys. Rev. A **88**, 032517 (2013).
[42] A. Raeber and D. A. Mazziotti, Large eigenvalue of the cumulant part of the two-electron reduced density matrix as a measure of off-diagonal long-range order, Phys. Rev. A **92**, 052502 (2015).
[43] O. Werba, A. Raeber, K. Head-Marsden, and D. A. Mazziotti, Signature of van der waals interactions in the cumulant density matrix, Phys. Chem. Chem. Phys. **21**, 23900 (2019).
[44] A. O. Schouten, L. M. Sager-Smith, and D. A. Mazziotti, Large cumulant eigenvalue as a signature of exciton condensation, Phys. Rev. B **105**, 245151 (2022).
[45] S. Donsa, F. Lackner, J. Burgdörfer, M. Bonitz, B. Kloss, A. Rubio, and I. Březinová, Nonequilibrium correlation dynamics in the one-dimensional Fermi-Hubbard model: A testbed for the two-particle reduced density matrix theory, Phys. Rev. Res. **5**, 033022 (2023).
[46] E. Majorana, Teoria simmetrica dell'elettrone e del positrone, Nuovo Cimento **14**, 171 (1937).